ChemComm

COMMUNICATION

View Article Online
View Journal | View Issue

Cite this: *Chem. Commun.*, 2018, **54**, 11649

Received 12th June 2018,
Accepted 21st September 2018

DOI: 10.1039/c8cc04642e

rsc.li/chemcomm

Activating 2D nano-kaolinite using hybrid nanoparticles for enhanced phosphate capture†

Yanfu Wei,[a] Peng Yuan,*[ab] Yaran Song,[ab] Dong Liu,[ab] Dusan Losic,[c] Daoyong Tan,[d] Fanrong Chen,[ab] Hongchang Liu,[a] Peixin Du[ab] and Junming Zhou[ab]

A synergistic host–guest coupling is exploited to disorder nano-kaolinite unit layers to form Al_2O_3 nanoparticles, which act as activated adsorptive sites; meanwhile, the coupling enables La-based nanoparticles to anchor homogenously on the nano-kaolinite surfaces, fully utilizing their adsorption ability. The activated hybrid nanostructures exhibit an excellent phosphate adsorption capacity.

Porous two-dimensional (2D) nanostructures have received considerable research attention in the adsorption field due to their large specific surface area, high mechanical stability, and easy surface modification and functionalization.[1,2] By loading or entrapping adsorptive nanomaterials on the substrate with 2D nanostructures, a variety of 2D nanohybrids have been created and shown to adsorb a broad range of pollutants with effectiveness.[3] Various modification strategies were utilized, including host–guest interactions such as hydrogen bonding,[4] layer-by-layer assembly,[5] covalent bonding,[6] and electrostatic attraction.[7] Usually, the 2D nanostructured hosts act as an inert support to immobilize adsorptive materials on their surfaces. Thus, 2D hosts such as graphene oxide[8] contribute little despite having a high cost of preparation. This largely limits the use of 2D nanohybrids in the removal of environmental pollutants, where great amounts of adsorbents are used and economic viability is of importance.

To tackle these challenges, we came with the concept to replace expensive synthetics with natural 2D nanostructures that are available at low cost from natural resources. We present a new synthetic strategy of 2D hybrid nanostructures coupling adsorptive nanoparticles and an activated natural 2D nanostructured host, where both contribute to the adsorption. The strategy is schematically shown in Fig. 1 and is shown to create double-face multifunctional 2D hybrid nanostructures providing high-performance adsorption of phosphate. A 2D layer nanoclay, nano-kaolinite ($Al_2Si_2O_5(OH)_4$; denoted as NKaol), served as an activated 2D nanostructured host. Lanthanum oxycarbonate ($La_2O_2CO_3$, abbreviated as LO) nanoparticles acted as the adsorptive guest. NKaol is a natural nanoclay, and it is readily available in large quantities as a low cost industrial material.[9] A unit layer of NKaol consists of an oxygen-sharing tetrahedral SiO_4 sheet and an adjacent octahedral AlO_6 sheet.[10] The unit layers are stacked up to form 2D layered NKaol with a gibbsite-like array of aluminol (Al–OH) groups on the octahedral surface and siloxane (Si–O–Si) groups on the tetrahedral surface.[11] Fig. 1 schematically represents the preparation of the nanohybrid. NKaol was first mixed with LO precursors ($La(NO_3)_3$ and $C_2H_5NO_2$). The mixture was further calcinated at 450 °C using the solution combustion method to obtain hybrid LO–NKaol (detailed in the ESI†). In the produced nanohybrid, LO nanoparticles were homogeneously anchored on the surfaces of NKaol; in the meantime, NKaol was activated by co-calcination with the coated LO precursors thus disconnecting the unit layers of NKaol and creating adsorptive Al_2O_3. The combined

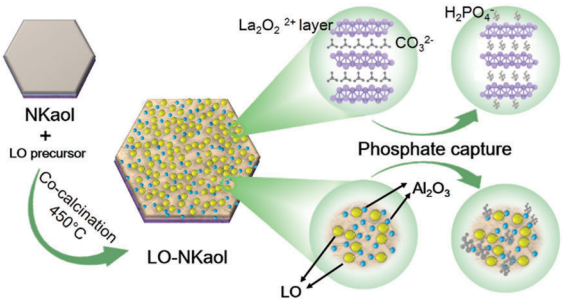

Fig. 1 Schematic illustration of creating 2D hybrid nanostructures by coupling NKaol and LO nanoparticles for enhanced uptake of phosphate from water.

[a] *CAS Key Laboratory of Mineralogy and Metallogeny/Guangdong Provincial Key Laboratory of Mineral Physics and Materials, Guangzhou Institute of Geochemistry, Chinese Academy of Sciences (CAS), Guangzhou 510640, China. E-mail: yuanpeng@gig.ac.cn*
[b] *University of Chinese Academy of Sciences, Beijing 100049, China*
[c] *School of Chemical Engineering, The University of Adelaide, Adelaide, South Australia 5005, Australia*
[d] *Key Laboratory of Solid Waste Treatment and Resource Recycle, Ministry of Education, Southwest University of Science and Technology, Mianyang 621010, China*

† Electronic supplementary information (ESI) available: Details of the synthesis of LO–NKaol, phosphate adsorption, and characterizations. See DOI: 10.1039/c8cc04642e

function of LO and Al_2O_3 accounts for a high phosphate adsorption capacity. Besides, the creation of LO–NKaol is facile *via* a bottom-up synthesis, and the strategy is economically viable because of using low-cost NKaol for adsorption.

The capability of this unique 2D hybrid nanostructure is revealed in the phosphate adsorption process. Phosphate pollution leads to eutrophication and threatens organisms in aquatic environments.[12] Over the past decade, Al, Fe, Zr and La-based metal (hydro) oxide adsorbents have been used for phosphate removal with effectiveness.[13] In particular, La-based compounds have a high capacity for removing phosphate and are one of the most efficient phosphate scavengers.[14] Various La-containing hybrids have been prepared for phosphate removal using porous hosts such as zeolite,[15] biochar,[16] graphene[17] and polyacrylonitrile nanofibers.[18] This was the rationale for our use of LO nanoparticles coated on the surface of 2D natural NKaol—it would synergistically uptake phosphate at Al_2O_3 and LO sites.

The successful coating of La-based nanoparticles on the surface of NKaol is confirmed by transmission electron microscopy (TEM) and scanning transmission electron microscopy (STEM) combined with energy-dispersive spectroscopy (EDS) mapping (Fig. 2). TEM and STEM results (Fig. 2a and b) showed the La-based nanoparticles loaded on the surface of NKaol. The cross-sectional TEM image (Fig. 2a) of an NKaol particle reveals that the thickness of the particle is approximately 33.1 nm, corresponding to 46 unit layers of kaolinite. This result is in agreement with the atomic force microscopy result of pristine NKaol, which showed that the thickness of NKaol particles is approximately 25–80 nm (Fig. S1, ESI†). Both characterizations indicate the 2D nano-scale of the employed kaolinite nanoclay. The corresponding EDS elemental mapping (Fig. 2c) confirms the homogenous coating of the La-containing material at the surface of NKaol. X-Ray Fluorescence (XRF) quantitative analysis of the LO–NKaol sample showed that the La content represents approximately 5.22% of the total elemental content by mole fraction, *i.e.* 28.24% of elemental La by mass is coated on the surface of LO–NKaol (Table S1, ESI†).

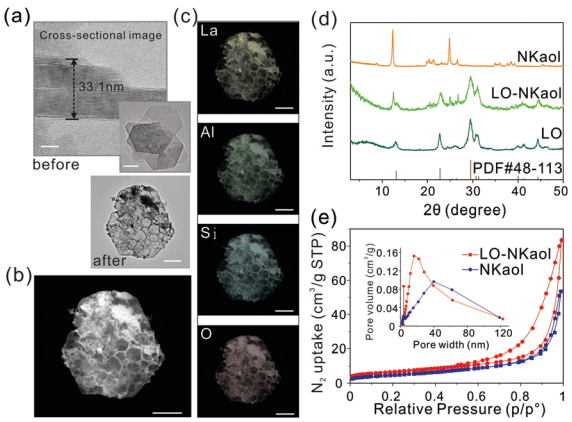

Fig. 2 (a) TEM images of NKaol before and after La coating, scale bars: 100 nm; the scale bar in the cross-sectional image of NKaol represents 10 nm. (b) STEM image of LO–NKaol and (c) corresponding quantitative EDS maps for La, Al, Si and O elements, scale bars: 200 nm. (d) XRD patterns of NKaol, LO and the resulting hybrid. (e) The nitrogen absorption–desorption isotherms and the corresponding pore size distribution (PSD) curves of NKaol and LO–NKaol.

As shown in Fig. 2d, the X-ray diffraction (XRD) patterns of the nanohybrid show that the main La-species is LO, because reflections of LO–NKaol with *d*-spacing values of 6.76, 3.90, 3.02, 2.90, 2.86, and 2.03 Å present characteristic diffraction of $La_2O_2CO_3$. The average diameter (*D*) of the LO crystallites is calculated using the Scherrer equation. The calculated *D* value is 7.8 nm. In addition, pristine calcinated NKaol exhibits a typical NKaol XRD pattern,[19] and the NKaol substrate in LO–NKaol presents a dramatically weakened intensity for the main reflections of NKaol, because (i) the calcination treatment at 450 °C caused the partial dehydroxylation of NKaol,[20] and (ii) LO reflection was introduced because of the LO coating. The nitrogen absorption–desorption isotherms of NKaol before and after LO coating were compared as shown in Fig. 2e. Both LO–NKaol and pristine calcinated NKaol are categorized as type II isotherms with H3 hysteresis loops as described by IUPAC.[21] This suggests that both materials belong to macroporous materials. Besides macropore domains, the PSD curve of NKaol shows a relatively broad pore population centered at 40 nm, revealing the occurrence of mesopores (Fig. 2e). The PSD curve of LO–NKaol exhibits higher mesopore populations with a unimodal shape with the centre peak at 16 nm. The possible reason was that the loading of La species on the external surface increases the interparticle mesopores. The BET specific surface area and the total pore volume values of LO–NKaol (23.9 $m^2\ g^{-1}$ and 0.09 $cm^3\ g^{-1}$) are larger than those of NKaol (17.2 $m^2\ g^{-1}$ and 0.06 $cm^3\ g^{-1}$, respectively). It is reasonable to infer that the coating of LO on the surfaces of NKaol increases the porosity of the materials.

Fourier transform infrared (FTIR) spectroscopy and X-ray photoelectron spectroscopy (XPS) results confirm the LO coating on the surface of NKaol (detailed in the ESI,† Fig. S2 and S3). In particular, the intensities of Al–OH vibrations in NKaol after LO coating (at 3695, 3622, and 914 cm^{-1})[22] decreased a lot when compared with those in pristine NKaol. This demonstrates that the LO coating leads to dehydroxylation and related structural changes of NKaol. Besides, the spectra of LO–NKaol show a heavy weakening of the Si–O vibrations (at 1100, 1032, 694 and 470 cm^{-1}) and Al–O–Si vibrations (538 and 754 cm^{-1}),[23] suggesting a disorder of the NKaol unit layer which includes tetrahedral SiO_4 and octahedral AlO_6. Thus, there is a phase separation of SiO_2 and Al_2O_3—both of which are amorphous nanoparticles.[19] These results show that co-calcination of NKaol and LO precursors leads to the disorder of the NKaol unit layer forming nanosized Al_2O_3. XPS results reveal the coating of LO on NKaol surfaces with Si–O–La and Al–O–La bonding which helps LO nanoparticles to further deposit at the surfaces of NKaol.

The efficiency of La–NKaol for removing phosphate from aqueous solutions has been examined by investigating the phosphate adsorption kinetics and isotherms. It was observed that the hybrid nanostructure removes phosphate quickly which can attain 80.8% of the adsorption capacity within 1 h, as shown in the adsorption kinetic curves (Fig. 3a). The adsorption behavior was well described by Langmuir isotherm models (Fig. 3b). Remarkably, the Langmuir maximum phosphate adsorption capacity of

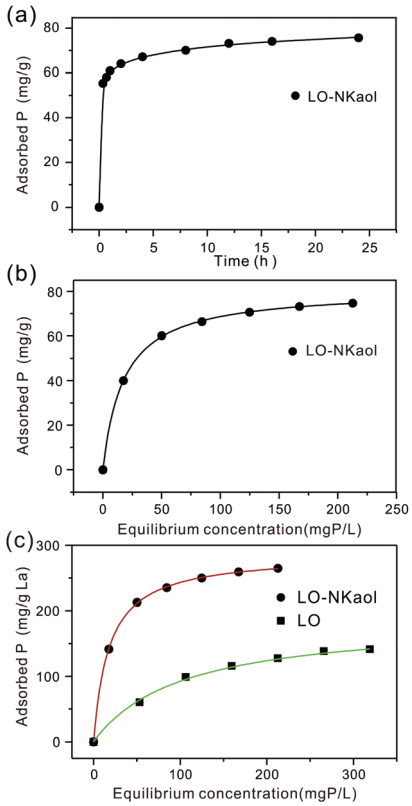

Fig. 3 (a) Phosphate adsorption kinetic curves of LO–NKaol. (b) Phosphate adsorption isotherms of LO–NKaol. (c) Comparison of the adsorption performance among LO–NKaol and pure LO nanoparticles. The adsorption isotherms in (b and c) are fitted using the Langmuir model.

LO–NKaol reaches up to 80.8 mgP g^{-1}. This value is higher than most of the reported phosphate adsorbents, *e.g.*, 8.28 mgP g^{-1} for zirconium phosphate,[24] 22 mgP g^{-1} for La-doped mesoporous silicates,[25] 44.8 mgP g^{-1} for La-decorated magnetite,[26] 46.4 mgP g^{-1} for La-composites coated biochar,[16] 71.9 mgP g^{-1} for lanthanum hydroxide/zeolite,[27] and 67.1 mgP g^{-1} for La(III) (hydr)oxide modified wheat straw[28] (see details in Table S2, ESI†). The phosphate adsorption capacity of LO–NKaol and LO were further compared *via* normalization of the La content (Fig. 3c). The as-prepared nanostructure showed a maximum phosphate uptake capacity of 286.3 mgP g^{-1} La, superior to pure LO (173.2 mgP g^{-1} La). And the control samples, uncalcined and calcined NKaol (450 and 700 °C) exhibit negligible phosphate adsorption (0.1, 1 and 0.5 mgP g^{-1} respectively, Table S3, ESI†). Hence, the low phosphate adsorption capacity of these control samples clearly indicates that the coupling of NKaol and LO nanoparticles accounts for the outstanding phosphate adsorption.

The FTIR and XPS analyses (detailed in the ESI†) confirm the multiple phosphate adsorption mechanisms and the possible synergetic adsorption by the individual components of the hybrid. FTIR spectra indicate the nearly complete replacement of the exchangeable CO_3^{2-} groups between $(La_2O_2^{2+})_n$ layers of LO in the hybrid by $H_2PO_4^-$, and the low CO_3^{2-}–$H_2PO_4^-$ exchange for the pure LO nanoparticles due to their aggregation (see Fig. S4, ESI†). Besides ion exchange adsorption, the XPS spectra confirm that

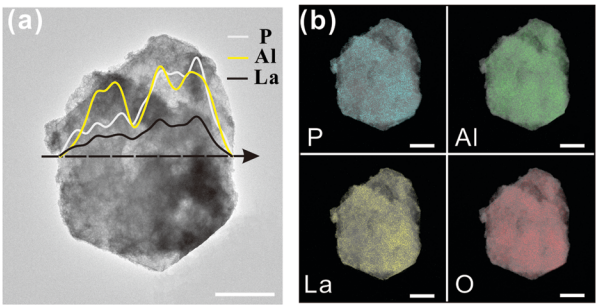

Fig. 4 (a) TEM images of P@LO–NKaol and EDS line scans along the black dotted line (the inset of the TEM image), and (b) elemental mapping for elements: P, Al, La and Si. Scale bars: 500 nm.

phosphate removal also occurs through surface complexation. This is due to the formation of the La–O–P bond and the Al–O–P bond at the surface of LO–NKaol, including the surface of LO and the activated Al_2O_3 nanoparticles.

TEM combined with EDS line-scanning and elemental mapping characterization (Fig. 4) identified elemental P dispersed at the surface of the phosphate-adsorbed LO–NKaol sample (P@LO–NKaol). The line scan data (the inset of the TEM image, Fig. 4a) reveal that elemental La and Al interact with P because of the correlation between the amount of P atoms and the number of La and Al atoms. This result implies that both LO and Al_2O_3 nanoparticles in LO–NKaol contribute to phosphate removal. In addition, the EDS mapping images (Fig. 4b) show homogeneous distribution of P at the surfaces of NKaol. Hence, these results clearly verify the coupling of the phosphate adsorption capacity of LO and Al_2O_3 in LO–NKaol.

Phosphorus K-edge X-ray absorption near-edge structure (XANES) analysis was used to identify the proportion of phosphorus adsorbed to the individual components of the LO–NKaol samples. Linear combination fitting (LCF) of the XANES spectrum for sample P@LO–NKaol was further conducted by using the spectra of phosphate adsorbed LO (P@LO) and phosphate adsorbed Al_2O_3 (P@Al_2O_3) as references (Fig. 5). The mean square misfit between the data and the model $\left(\sum_j (\mathrm{data}_j - \mathrm{fit}_j) \Big/ \sum_j \mathrm{data}^2\right)$, defined as the *R*-factor, represents the fit quality in LCF analysis. Usually, the value of *R*-factor is below 0.05 displaying a good LCF fit; and the smaller the *R*-factor is, the better the fit.[29] The LCF analysis shows that the proportion of phosphate adsorbed to LO and Al_2O_3 in the hybrid was 90% and 10%, respectively. Moreover, the corresponding *R*-factor of the LCF fitting is 0.001003, showing a high-quality fitting. These results resonate with the combination of both LO and Al_2O_3 in the hybrid in uptaking phosphate.

The high adsorption performance of LO–NKaol nanostructures is achieved by the combined characteristics of the two components (schematically shown in Fig. 1): (1) Co-calcination of NKaol and LO precursors leads to the disordering of the original tetrahedral SiO_4 and octahedral AlO_6 sheets of NKaol and formation of amorphous Al_2O_3 nanoparticles that act as an additional component for phosphate removal. Meanwhile, the neglectable phosphate adsorption capacity of the calcinated NKaol samples suggests that calcination of NKaol at 450 and 700 °C did not produce active

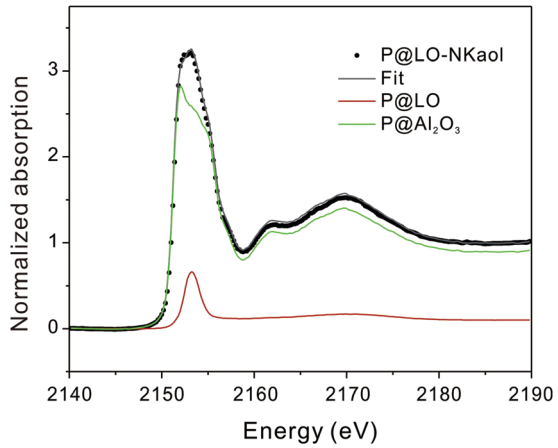

Fig. 5 LCF analysis of phosphorus XANES spectra of the P@LO–NKaol samples (the scattering dots). The black line is the resultant spectrum by fitting the spectra of the P@LO (the green line) and P@Al_2O_3 (the red line) references.

Al_2O_3; (2) the special 2D layer nanostructure of NKaol and its tunable surface properties enable LO nanoparticles to deposit homogenously and covalently on the surfaces allowing maximum phosphate removal. However, the pure LO particles tend to aggregate, showing limited adsorption performance.

The LO–NKaol material is affordable and easy to produce. Bottom-up LO–NKaol adsorbents are produced through solution combustion synthesis at a relatively low temperature (450 °C), and they can easily be produced in a large quantity from one batch of synthesis. Moreover, the raw kaolinite mineral to produce NKaol is about six times cheaper than graphite which is used to produce 2D graphene-based materials.[30] Furthermore, the LO nanoparticles are stable and are strongly anchored on NKaol. What is more, various adsorptive nanoscale materials can be coated on NKaol surfaces *via* solution combustion synthesis to activate NKaol and create novel adsorbent materials. As Al_2O_3 nanoparticles are widely used adsorbents for the removal of various pollutants in water treatment,[31] the coupling of adsorptive nanomaterials and activated NKaol creates a potential of high adsorption capacity for various pollutants.

In conclusion, we show here a unique 2D hybrid nanostructure by using natural NKaol and LO nanoparticles. This product offers efficient removal of phosphate from aqueous solutions and a high adsorption capacity of 80.8 mgP g^{-1} was achieved. The composite is synthesized by coating LO nanoparticles on the activated NKaol structure, to make them available for phosphate adsorption due to the formation of amorphous Al_2O_3 from disconnection of the unit layer of NKaol. Adsorption occurs on LO and Al_2O_3 sites aided by the unique geometry of the NKaol layer nanostructures. Well-dispersed LO nanoparticles are covalently anchored on the NKaol surfaces, and they increase the efficiency of La for phosphate adsorption. LO–NKaol has a higher adsorption ability than LO particles alone. By combining easy preparation, low cost, and high stability, the 2D hybrid complexes offer significant promise for phosphate capture from polluted water. The concept for the creation of the novel nanostructure by activating NKaol is potentially applicable to various adsorptive metal oxides. And these hybrid nanocomposites may be a new generic platform for effective scavenging of various pollutants.

This work is supported by the National Natural Science Foundation of China (Grant No. 41472045, 41672042, and 41603118), a grant from the Youth Innovation Promotion Association CAS for the excellent members (2016-81-01), the CAS President's International Fellowship Initiative for Visiting Scientists (Grant No. 2017VEA0009), and the Open Funds of the Beijing Synchrotron Radiation Facility (No. 2017-BEPC-PT-001052 and 2017-BEPC-PT-001065). This is a contribution No. IS-2589 from the GIGCAS.

Conflicts of interest

There are no conflicts to declare.

Notes and references

1 Q. Fu and X. Bao, *Chem. Soc. Rev.*, 2017, **46**, 1842–1874.
2 R. Cui, Y. Lin, J. Qian, Y. Zhu, N. Xu, F. Chen, C. Liu, Z. Wu, Z. Chen and X. Zhou, *ACS Sustainable Chem. Eng.*, 2017, **5**, 3478–3487.
3 A. Jana, E. Scheer and S. Polarz, *Beilstein J. Nanotechnol.*, 2017, **8**, 688–714.
4 W. Wei, G. Wang, S. Yang, X. Feng and K. Müllen, *J. Am. Chem. Soc.*, 2015, **137**, 5576–5581.
5 J. Shen, Y. Hu, C. Li, C. Qin, M. Shi and M. Ye, *Langmuir*, 2009, **25**, 6122–6128.
6 F. He, J. Fan, D. Ma, L. Zhang, C. Leung and H. L. Chan, *Carbon*, 2010, **48**, 3139–3144.
7 X. Long, J. Li, S. Xiao, K. Yan, Z. Wang, H. Chen and S. Yang, *Angew. Chem., Int. Ed.*, 2014, **53**, 7584–7588.
8 S. Sakulpaisan, T. Vongsetskul, S. Reamouppaturm, J. Uangkachao, J. Tantirungrotechai and P. Tangboriboonrat, *J. Environ. Manage.*, 2016, **167**, 99–104.
9 Z. Yan, L. Fu and H. Yang, *Adv. Mater. Interfaces*, 2018, **5**, 1700934.
10 L. Mei, Z. Yi, H. Peng, C. Shi, H. Yuehua, Y. Qian, M. Linfeng and Y. Huaming, *Adv. Funct. Mater.*, 2017, **28**, 1704452.
11 P. Yuan, D. Tan, F. Annabi-Bergaya, W. Yan, D. Liu and Z. Liu, *Appl. Clay Sci.*, 2013, **83–84**, 68–76.
12 D. J. Conley, H. W. Paerl, R. W. Howarth, D. F. Boesch, S. P. Seitzinger, K. E. Havens, C. Lancelot and G. E. Likens, *Science*, 2009, **323**, 1014–1015.
13 Y.-T. Liu and D. Hesterberg, *Environ. Sci. Technol.*, 2011, **45**, 6283–6289.
14 J. He, W. Wang, F. Sun, W. Shi, D. Qi, K. Wang, R. Shi, F. Cui, C. Wang and X. Chen, *ACS Nano*, 2015, **9**, 9292–9302.
15 Z. Wang, Y. Fan, Y. W. Li, F. R. Qu, D. Y. Wu and H. N. Kong, *Microporous Mesoporous Mater.*, 2016, **222**, 226–234.
16 Z. H. Wang, D. K. Shen, F. Shen and T. Y. Li, *Chemosphere*, 2016, **150**, 1–7.
17 M. Chen, C. Huo, Y. Li and J. Wang, *ACS Sustainable Chem. Eng.*, 2016, **4**, 1296–1302.
18 J. J. He, W. Wang, W. X. Shi and F. Y. Cui, *RSC Adv.*, 2016, **6**, 99353–99360.
19 N. Worasith, B. A. Goodman, J. Neampan, N. Jeyachoke and P. Thiravetyan, *Clay Miner.*, 2016, **46**, 539–559.
20 H. Peng, J. Vaughan and J. Vogrin, *Appl. Clay Sci.*, 2018, **157**, 189–197.
21 S. J. Gregg and K. S. W. Sing, *Adsorption, surface area, and porosity*, Academic Press, 1982.
22 A. K. Panda, B. G. Mishra, D. K. Mishra and R. K. Singh, *Colloids Surf., A*, 2010, **363**, 98–104.
23 C. Bich, J. Ambroise and J. Péra, *Appl. Clay Sci.*, 2009, **44**, 194–200.
24 Q. Zhang, Q. Du, T. Jiao, B. Pan, Z. Zhang, Q. Sun, S. Wang, T. Wang and F. Gao, *Chem. Eng. J.*, 2013, **221**, 315–321.
25 J. Zhang, Z. Shen, W. Shan, Z. Chen, Z. Mei, Y. Lei and W. Wang, *J. Environ. Sci.*, 2010, **22**, 507–511.
26 H. Fu, Y. Yang, R. Zhu, J. Liu, M. Usman, Q. Chen and H. He, *J. Colloid Interface Sci.*, 2018, **530**, 704–713.
27 J. Xie, Z. Wang, D. Fang, C. Li and D. Wu, *J. Colloid Interface Sci.*, 2014, **423**, 13–19.
28 H. Qiu, C. Liang, J. Yu, Q. Zhang, M. Song and F. Chen, *Chem. Eng. J.*, 2017, **315**, 345–354.
29 S. Liu, C. Jing and X. Meng, *Sci. Total Environ*, 2008, **392**, 137–144.
30 H. Cheng, Y. Zhou, Y. Feng, W. Geng, Q. Liu, W. Guo and L. Jiang, *Adv. Mater.*, 2017, **29**, 1700177.
31 J. S. Yamani, A. W. Lounsbury and J. B. Zimmerman, *Water Res.*, 2014, **50**, 373–381.

